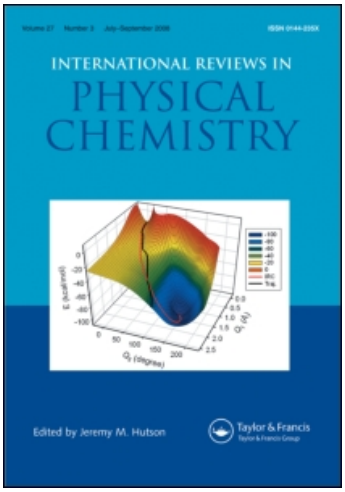

International Reviews in Physical Chemistry
Publication details, including instructions for authors and subscription information:
http://www.informaworld.com/smpp/title~content=t713724383

Path integral simulations of atomic and molecular systems

Charusita Chakravarty

Online publication date: 26 November 2010

To cite this Article Chakravarty, Charusita(1997) 'Path integral simulations of atomic and molecular systems', International Reviews in Physical Chemistry, 16: 4, 421 — 444
To link to this Article: DOI: 10.1080/014423597230190
URL: http://dx.doi.org/10.1080/014423597230190

INTERNATIONAL REVIEWS IN PHYSICAL CHEMISTRY , 1997, VOL. 16, NO. 4. 421–444

Path integral simulations of atomic and molecular systems

By CHARUSITA CHAKRAVARTY

Department of Chemistry, Indian Institute of Technology–Delhi, Hauz Khas, New Delhi 110016, India

The path integral picture of the statistical mechanics of quantum many-body systems is presented from the point of view of developing simulation algorithms. Monte Carlo and molecular dynamics techniques for systems of distinguishable quantum particles, bosons and fermions are reviewed. Path integral simulations of atomic liquids and solids, quantum clusters and solvated electrons are described and the usefulness of such techniques for understanding phenomena such as orientational transitions, surface adsorption and rates of quantum processes is discussed.

1. Introduction

Quantum Monte Carlo (QMC) methods are stochastic simulation methods for quantum many-body systems. In terms of computational cost, Monte Carlo methods scale very favourably with system size and have played a crucial role in understanding the statistical mechanics of classical many-body systems since the 1940s [1–3]. Monte Carlo methods for quantum many-body systems are of more recent vintage and fall into two very different categories: (a) the zero-temperature or ground state methods such as variational and diffusion Monte Carlo and (b) the finite temperature path integral (PI) simulation methods which provide equilibrium properties within the canonical ensemble [4–10]. This review focuses on the formalism and methodology of PI simulations as applicable to atomic and molecular systems with continuous potentials.

Quantum effects in chemical systems can arise from quantization of either electronic or nuclear motion. Standard electronic techniques rely on variational optimization of a wavefunction constructed as a linear combination of one-electron functions; inherently many-body effects such as electron correlation are then difficult to capture for all but the smallest molecules [11]. Density functional approaches, which are restricted to the ground state but include electron correlation approximately, are preferred for extended systems [12]. QMC methods being inherently correlated many-body approaches that, in principle, do not involve any approximations should therefore correct for the deficiencies of both basis set and density functional methods. While QMC methods are exact, within statistical error, for systems of distinguishable quantum particles and for bosons, they suffer from the well known 'sign' problem for fermionic systems, discussed in sections 2.2 and 3.4, which must be circumvented by introducing some approximations. Despite this limitation, recent work shows that for many systems, including carbon and silicon clusters, QMC methods achieve chemical accuracy [7, 8]. Since most applications to electronic structure have involved zero-temperature simulations, they are not included in this review. We concentrate instead on systems containing light nuclei at low temperatures. Quantum effects in such systems can vary from the quasiclassical limit in solid argon to the extreme quantum limit exemplified by superfluid helium [2, 3]. Many solids such as ammonium halides, solid H_2 and hydrogen-bonded solids show phase transitions with large isotope effects indicative of strong quantum effects [13]. Electron and proton transfer, vital to many

0144–235X/97 $12·00

biochemical processes, are intrinsically quantum mechanical [14]. The influence of quantum effects on the structure and dynamics of water clusters is well documented [15]. The finite temperature properties of such systems can be obtained from PI simulations.

The PI formulation of quantum mechanics was originally developed by Feynman and applied to quantum electrodynamics and statistical mechanics [16–18]. In the context of statistical mechanics, this formulation allows the quantum mechanical partition function of a system to be written as a much higher dimensional classical partition function with a modified potential energy function. This quantum classical isomorphism was used, for example, by Feynman to show that the hard sphere bosonic fluid would undergo Bose–Einstein condensation. The possibility that the quantum classical isomorphism would allow Metropolis Monte Carlo simulations for quantum systems, similar to those used for classical liquids, was first suggested by Morita [19] and later by Barker [20]. The implications for atomic systems were developed by D. Chandler, P. G. Wolynes and co-workers [14, 21, 22]. The first PI simulations of realistic atomic systems were for two apparently very different physical problems: the F-centre formed by an electron trapped in an alkali halide lattice [23, 24] and liquid helium in the region of the superfluid transition [25]. In the past fifteen years, applications to a variety of atomic and molecular systems have been made. An overview of the methods found to be most useful for chemical systems is presented here.

The review is organized as follows. Section 2 discusses the PI formulation of the density matrix from the point of view of developing computational algorithms. Monte Carlo implementations of the PI formalism for distinguishable particles, bosons and fermions are described in section 3. Dynamical, instead of stochastic, sampling strategies for PI simulations are reviewed briefly in section 4. Section 5 presents some applications of the path integral Monte Carlo (PIMC) method to atomic and molecular systems which have been selected to demonstrate how the technique can be adapted to study a variety of interesting physical problems. Section 6 contains conclusions.

2. Path integral formulation of the density matrix

2.1. *The quantum-classical isomorphism*

The thermal density matrix describes the properties of a quantum system in the canonical ensemble and may be defined as [18]

$$\hat{\rho} = \sum_n \exp(-\beta E_n) |\phi_n\rangle\langle\phi_n| \tag{1}$$

where $\{|\phi_n\rangle\}$ are eigenfunctions of the Hamiltonian $\hat{H}$ with eigenvalues $\{E_n\}$, $\beta = k_B T$, k_B is the Boltzmann constant and T is the absolute temperature. The partition function Z of the system is given by

$$Z = \sum_n \exp(-\beta E_n) = \sum_n \langle\phi_n|\hat{\rho}|\phi_n\rangle = \mathrm{Tr}\{\hat{\rho}\}. \tag{2}$$

The PI formulation of the density matrix can be developed by considering the coordinate representation of Z for a single quantum particle of mass m subject to a potential $V(x)$ [26, 27]. Then Z is an integral over diagonal elements of the density matrix

$$Z = \int \mathrm{d}x \langle x | \exp(-\beta\hat{H}) | x \rangle \tag{3}$$

and $\exp(-\beta\hat{H})$ may be interpreted as the propagator in imaginary time, $t = \mathrm{i}\beta\hbar$. $\hat{H}$ is the sum of the kinetic $\hat{K}$ and potential $\hat{V}$ energy operators. Writing $\exp(-\beta\hat{H}) = [\exp(-(\beta/M)\hat{H})]^M$ and inserting $M-1$ complete sets of coordinate states $\{|x_j\rangle\}, j = 1$ to $M-1$, between the M high temperature density operators, we get

$$Z = \int \prod_{i=0}^{M-1} \mathrm{d}x_i \left\langle x_i \left| \exp\left(-\frac{\beta}{M}\hat{H}\right) \right| x_{i+1} \right\rangle \tag{4}$$

where $x_0 = x_M = x$ because of the trace operation associated with the partition function. Provided $\varepsilon = \beta/M$ is sufficiently small, one can make the following power series expansion

$$\exp(-\varepsilon\hat{H}) = \exp(-\varepsilon\hat{K}) \exp(-\varepsilon\hat{V}) + \exp(-0{\cdot}5\varepsilon^2[\hat{K}, \hat{V}]) + \ldots . \tag{5}$$

Ignoring all correction terms of order ε^2 and above in the exponent leads to the Trotter approximation [27]

$$\exp(-\beta\hat{H}) = \lim_{M\to\infty} [\exp(-\varepsilon\hat{K}) \exp(-\varepsilon\hat{V})]^M. \tag{6}$$

The high temperature density matrix elements are then given by

$$\rho(x_i, x_{i+1}; \varepsilon) = \langle x_i | \exp(-\varepsilon\hat{H}) | x_{i+1} \rangle = \langle x_i | \exp(-\varepsilon\hat{K}) | x_{i+1} \rangle \exp(-\varepsilon V(x_{i+1})). \tag{7}$$

Since $\hat{K} = \hat{p}^2/2m$ where $\hat{p}$ is the momentum operator, by inserting a complete set of momentum states $\{|p\rangle\}$ we obtain

$$\begin{aligned}
\rho(x_i, x_{i+1}; \varepsilon) &= \int \mathrm{d}p \left\langle x_i \left| \exp\left(-\frac{\varepsilon\hat{p}^2}{2m}\right) \right| p \right\rangle \langle p | x_{i+1} \rangle \exp(-\varepsilon V(x_{i+1})) \\
&= \int \frac{\mathrm{d}p}{2\pi\hbar} \exp\left(-\frac{\varepsilon p^2}{2m}\right) \exp(\mathrm{i}p(x_i - x_{i+1})/\hbar) \exp(-\varepsilon V(x_{i+1})) \\
&= \left(\frac{m}{2\pi\varepsilon\hbar^2}\right)^{1/2} \exp\left(-\frac{m(x_i - x_{i+1})^2}{2\varepsilon\hbar^2}\right) \exp(-\varepsilon V(x_{i+1})).
\end{aligned} \tag{8}$$

The above approximation to the high temperature density matrix is frequently referred to as the primitive approximation. If it is necessary to apply periodic boundary conditions on a box of length L, the momentum states must be restricted to integer multiples of $2\pi/L$; however, the above formula will be very nearly exact if the thermal de Broglie wavelength at inverse temperature β/M is much less than L [6]. Substituting the semiclassical expression for the high temperature density matrix element from equation (8) in equation (4) leads to

$$Z = \left(\frac{m}{2\pi\varepsilon\hbar^2}\right)^{M/2} \int \left(\prod_{i=0}^{M-1} \mathrm{d}x_i \right) \exp\left(-\frac{m}{2\varepsilon\hbar^2} \sum_{i=0}^{M-1} (x_i - x_{i+1})^2 - \varepsilon \sum_{i=0}^{M-1} V(x_i) \right). \tag{9}$$

The position coordinates of the system at equispaced points in imaginary time u between 0 and $\beta\hbar$ are given by $\{x_i\}, i = 0$ to M, where $x = x_0 = x_M$. In the limit $\varepsilon \to 0$, when errors due to the Trotter approximation vanish, the exponent in equation (9) becomes exactly equal to the Euclidean action $S(x(u))$ along an imaginary time path $x(u)$ such that

$$S(x(u)) = (1/\hbar) \int_0^{\beta\hbar} \left(\frac{m}{2} \left[\frac{\mathrm{d}x}{\mathrm{d}u} \right]^2 + V(x(u)) \right) \mathrm{d}u. \tag{10}$$

The density matrix element can then be written as a path integral

$$\langle x|\exp(-\beta\hat{H})|x'\rangle = \int \mathscr{D}(x(u))\exp(-S(x(u))) \tag{11}$$

where $\mathscr{D}(x(u))$ represents the differential element for all paths with the common starting point x and end point x'; for cyclic paths $x = x'$. The exponential weighting factor ensures that paths with very high values of action contribute much less than paths with low action. Such high action paths may be jagged paths with high kinetic energy or paths which access regions of high potential energy. It can be shown that if $\gamma\hbar$ is small, then the classical Boltzmann weighting factor, $\exp(-\beta V(x))$, is recovered [17]. Applying the continuum limit to equation (9) implies that the partition function will correspond to a PI over cyclic paths with all possible starting points. All PI simulation methods are techniques for sampling the physically important paths contributing to the partition function.

To understand how Metropolis Monte Carlo and molecular dynamics techniques, originally developed for classical systems, can be adapted to simulate a quantum many-body system, it is necessary to go back to equation (9). The expression for Z can be interpreted as the partition function of a classical polymer of M monomeric units or beads with adjacent beads linked by harmonic springs with force constant $mM/\beta\hbar^2$. The generalization of equation (9) to the case of N interacting, distinguishable quantum particles with Trotter number M in three dimensions is obvious:

$$Z_{NM} = \left(\frac{m}{2\pi\varepsilon\hbar^2}\right)^{3NM/2} \int \left(\prod_{i=0}^{M-1} \mathrm{d}\mathbf{x}_i\right) \exp\left[\frac{-m}{2\varepsilon\hbar^2}\sum_{i=0}^{M-1}(\mathbf{x}_i - \mathbf{x}_{i+1})^2 - \varepsilon\sum_{i=0}^{M-1} V(\mathbf{x}_i)\right] \tag{12}$$

where the vector $\mathbf{x}_i$ denotes the $3N$ Cartesian coordinates of the N particles at time slice i. Each quantum particle is represented by a cyclic polymer of M beads. Beads on two separate cyclic polymers are coupled by the interaction $V(\mathbf{x})$ only if they lie on the same time slice. Adjacent beads on the same polymer are coupled by a harmonic interaction with force constant $m/\varepsilon\hbar^2$. The root mean square radius of the cyclic polymers is related to the degree of the quantum dispersion and will depend on the de Broglie wavelength of the particles as well as the interaction potential. The conversion of the N-dimensional quantum partition function to an NM-dimensional classical-type partition function by the introduction of $N(M-1)$-auxilliary variables to represent quantum paths in imaginary time is often referred to as the quantum classical isomorphism. From a computational point of view, this isomorphism implies that with any configuration of the derived classical system, a Boltzmann-type weight can be associated and therefore multidimensional integration techniques such as Metropolis Monte Carlo sampling can be applied. In general, the more quantum mechanical the system the greater the number of auxilliary variables per degree of freedom that is required for accuracy. Therefore the dimensionality and computational cost of a PI simulation is generally much higher than that of the corresponding classical system.

2.2. *Identical particles*

The above derivation of the PI representation of the partition function takes into account deviations from classical behaviour owing to quantum delocalization but neglects the effect of identical particle exchange. When the thermal de Broglie wavelength is of the same order of magnitude as the interparticle spacing, the bosonic or fermionic character of the constituents must be accounted for. Formally, this leads to a very simple modification of the result for a collection of distinguishable particles.

Let the density matrix for N distinguishable particles be labelled by D and for N indistinguishable particles by I. Then

$$\rho_{\mathrm{I}}(\mathbf{x}, \mathbf{x}'; \beta) = (1/N!) \sum_P \xi^P \rho_{\mathrm{D}}(\mathbf{x}, P\mathbf{x}'; \beta) \tag{13}$$

where P is the parity of the permutation and ξ is $+1$ for bosons and -1 for fermions [18, 26]. The effect of permutation P on the elements of the vector $\mathbf{x} = (x_1, x_2, \ldots x_N)$ is denoted by $P\mathbf{x}$. ξ^P is always $+1$ for bosons but for fermions it equals -1 and $+1$ for odd and even permutations respectively. $\rho_{\mathrm{D}}(\mathbf{x}, P\mathbf{x}'; \beta)$ can of course be written as a sum over paths, weighted by the exponential of the Euclidean action, with initial point $\mathbf{x}$ and final point $P\mathbf{x}'$ (see equation (11)). Therefore the density matrix element for indistinguishable particles can be written as

$$\rho_{\mathrm{I}}(\mathbf{x}, \mathbf{x}'; \beta) = (1/N!) \sum_P \xi^P \int_0^{\beta\hbar} \mathscr{D}(\mathbf{x}_{\mathrm{P}}(u)) \exp(-S(\mathbf{x}_{\mathrm{P}}(u)) \tag{14}$$

where the subscript P indicates that the final endpoint of the path is subject to the appropriate permutation. Consequently, instead of summing over only cyclic paths to obtain the partition function, as in the case of distinguishable particles, it becomes necessary to sample over all paths which end with permutational variations of the starting point.

The free particle case, for which the diagonal elements of density matrix are given by

$$\rho_{\mathrm{fp}}(\mathbf{x}, \mathbf{x}'; \beta) = \sum_P \xi^P \prod_{i=1}^{3N} \left(\frac{m}{2\pi\beta\hbar^2}\right)^{1/2} \exp[-(m/2\beta\hbar^2)(x_i - Px_i)^2], \tag{15}$$

illustrates qualitatively the importance of permutations for identical particle systems as a function of temperature. In the high temperature limit, $\beta \to 0$, only the identity permutation will survive. On the other hand, when $\beta \to \infty$, all permutations will be equally probable. At intermediate temperatures, the identity permutation will have maximum probability, followed by pair exchanges, and then higher order permutations.

For bosons, this implies that sampling over the discrete set of permutations is necessary but since the all permutations have positive weights, this causes no problems in principle. In the context of the quantum classical isomorphism, permutational exchanges of bosons are equivalent to cross-linking of the quantum polymers. For example, a pair exchange implies that the endpoints of two cyclic polymers are interchanged to form a larger single polymer. Superfluidity is then associated with the formation of a cross-linked polymer of macroscopic dimensions. The path integral picture for bosonic superfluids has been recently reviewed by Ceperley [6]. In contrast to bosonic systems, fermionic systems are problematic since the negative weights of odd permutations imply that a positive weight function for Monte Carlo sampling cannot always be defined. Consequently the statistical accuracy decreases sharply with temperature and gives rise to the fermion sign problem mentioned in the introduction [10].

2.3. Ab initio *path integral methods*

Simulation methods which combine a PI representation for the nuclei with standard electronic structure techniques have been developed recently for systems with light nuclei where interatomic interactions cannot be readily parametrized in terms of few-body interactions [28–35]. Since electronic structure calculations assume a

Schrödinger type picture and calculate the adiabatic Born–Oppenheimer (BO) electronic states, this section shows how the BO approximation is implemented within the PI picture and suggests how non-adiabatic corrections to the BO approximation can be incorporated [32, 37, 38].

The Hamiltonian for a molecular system can be written as:

$$\hat{H} = \hat{T}_n + \hat{T}_e + \hat{V}_{nn} + \hat{V}_{ne} + \hat{V}_{ee} \tag{16}$$

where $\hat{T}_e$ and $\hat{T}_n$ are the kinetic energy operators for the electrons and nuclei respectively and $\hat{V}_{nn}$, $\hat{V}_{ee}$ and $\hat{V}_{ne}$ are the potential energy operators for the internuclear, interelectronic and nuclear–electronic interactions. The electronic Hamiltonian $\hat{H}_e$ is defined as $\hat{H}_e = \hat{T}_e + \hat{V}_{ne} + \hat{V}_{ee}$, which depends only parametrically on the nuclear configuration $\mathbf{R}$. The BO electronic wavefunctions $\phi_e(\mathbf{r};\mathbf{R})$ are eigenfunctions of $\hat{H}_e$ such that $\hat{H}_e \phi_e = V_e(\mathbf{R})\phi_e$ where $\mathbf{r}$ stands for the electronic coordinates and the function $V_e(\mathbf{R})$ represents the potential energy surface on which the nuclei move in a given electronic state. The partition function for this system is $Z = \mathrm{Tr}(\exp\{-\beta\hat{H}\})$. While the conventional PI representation would require expanding this trace in the coordinate basis, $|\mathbf{r}\rangle|\mathbf{R}\rangle$, as done in [32], it is more convenient to use the mixed basis $|\phi\rangle|\mathbf{R}\rangle$. Then,

$$Z = \int d\mathbf{R} \sum_\alpha \langle \mathbf{R}|\langle \phi_\alpha|\exp\{-\beta(\hat{H}_e + \hat{H}_n)\}|\phi_\alpha\rangle|\mathbf{R}\rangle \tag{17}$$

where α labels the BO electronic states and $\hat{H}_n = \hat{T}_n + \hat{V}_{nn}$. Using the Trotter approximation, we can write

$$Z = \int d\mathbf{R} \sum_\alpha \langle \mathbf{R}|\langle \phi_\alpha|[\exp\{-\varepsilon(\hat{H}_e + \hat{H}_n)\}]^M|\phi_\alpha\rangle|\mathbf{R}\rangle \tag{18}$$

where $\varepsilon = \beta/M$. Inserting $M-1$ complete set of states $|\mathbf{X}_j\rangle = |\mathbf{R}_j\rangle|\phi_{\alpha(j)}\rangle$ results in

$$\int\left(\prod_j d\mathbf{R}_j\right)\sum_{\alpha(1)}\sum_{\alpha(2)}\cdots\sum_{\alpha(M)} \rho(\mathbf{X},\mathbf{X}_1;\varepsilon)\,\rho(\mathbf{X}_1,\mathbf{X}_2;\varepsilon)\cdots\rho(\mathbf{X}_{M-1},\mathbf{X};\varepsilon) \tag{19}$$

where

$$\rho(\mathbf{X}_i,\mathbf{X}_j;\varepsilon) = \langle \mathbf{R}_j|\langle \phi_{\alpha(j)}|\exp\{-\varepsilon(\hat{H}_n + \hat{H}_e)\}|\phi_{\alpha(j)}\rangle|\mathbf{R}_j\rangle. \tag{20}$$

Since $\phi_{\alpha(j)}$ is an eigenfunction of $\hat{H}_e$ such that the corresponding eigenvalue $V_{\alpha(j)}(\mathbf{R})$ can be regarded as the coordinate representation of the potential energy operator for the nuclei, we can write therefore

$$\rho(\mathbf{X}_i,\mathbf{X}_j;\varepsilon) = \langle \mathbf{R}_j|\langle \phi_{\alpha(j)}|\exp(-\varepsilon\hat{T}_n)|\phi_{\alpha(i)}\rangle|\mathbf{R}_i\rangle\exp(-\varepsilon(V_{\alpha(i)}(\mathbf{R}_i) + V_{nn}(\mathbf{R}_i))). \tag{21}$$

The matrix element $\langle \phi_{\alpha(j)}|\exp(-\varepsilon\hat{T}_n)|\phi_{\alpha(i)}\rangle$ can be expanded as

$$\langle \phi_{\alpha(j)}|\exp(-\varepsilon\hat{T}_n)|\phi_{\alpha(i)}\rangle = \langle \phi_{\alpha(j)}|1 - \varepsilon\hat{T}_n + 0{\cdot}5\varepsilon^2\hat{T}_n^2 + \ldots|\phi_{\alpha(i)}\rangle. \tag{22}$$

The BO approximation implies that the nuclear kinetic energy operator cannot couple different BO electronic states i.e. the above matrix element is unity when $\alpha(i) = \alpha(j)$ and zero otherwise. This implies that transitions between BO states will not take place along the path in imaginary time and the partition function will consist of separate sums over paths belonging to individual BO electronic states. Therefore, within the primitive approximation, Z may be written as

$$Z = \sum_\alpha \int\left(\prod_j d\mathbf{R}_j\right)\exp\left\{-\frac{m_n}{2\varepsilon\hbar^2}(\mathbf{R}_i - \mathbf{R}_j)^2 - \varepsilon V_\alpha(\mathbf{R}_i) - \varepsilon V_{nn}(\mathbf{R}_i)\right\} \tag{23}$$

where m_n is the nuclear mass. *Ab initio* PI simulations to date have used density

functional approaches for the electronic structure and therefore have been restricted to the BO ground state. Weak non-adiabatic effects can be incorporated by keeping the first order correction term in equation (22). This requires parametrization of the off-diagonal matrix elements of the operator $\hat{T}_n$ connecting two different BO states which is currently feasible only for very simple molecular systems.

2.4. *Observables*

In this section, we discuss the observables that can be evaluated in PI simulations [6]. The canonical ensemble average of an observable O is given by

$$\langle O \rangle = \mathrm{Tr}\{\hat{\rho}\hat{O}\}/\mathrm{Tr}\{\hat{\rho}\} \tag{24}$$

where $\hat{O}$ is the corresponding quantum mechanical operator. If the operator $\hat{O}$ is diagonal in the coordinate representation, then

$$\langle O \rangle = \int \mathrm{d}\mathbf{x} O(\mathbf{x})\, \rho(\mathbf{x}, \mathbf{x}; \beta). \tag{25}$$

Provided a technique exists for sampling configurations $\mathbf{x}$ with probability proportional to $\rho(\mathbf{x}, \mathbf{x}; \beta)$, such equilibrium averages can be readily calculated. As we shall see in sections 3 and 4, Monte Carlo and, under more restricted conditions, molecular dynamics, provide efficient routes to implement this type of sampling. Static equilibrium averages, such as the potential energy or position–position correlation functions, are the most easily accessible quantities from a PI simulation. In addition, dynamical variables that can be related to the partition function are straightforward to obtain. Within the canonical ensemble, thermodynamic estimators of the total energy $\langle E \rangle$, the kinetic energy $\langle K \rangle$, the specific heat C_v and the pressure $\langle P \rangle$ can be derived from Z as

$$\langle E \rangle = -\frac{\partial(\ln Z)}{\partial \beta}, \tag{26}$$

$$\langle K \rangle = \frac{m}{\beta}\frac{\partial(\ln Z)}{\partial m}, \tag{27}$$

$$C_v/k_B = -\beta^2 \frac{\partial^2(\ln Z)}{\partial \beta^2}, \tag{28}$$

$$\langle P \rangle = (1/\beta)\frac{\partial(\ln Z)}{\partial V}. \tag{29}$$

The above expression for $\langle K \rangle$ will be applicable only when all particles in the system have the same mass. An alternative method of estimating the kinetic energy is obtained from the virial theorem and is given by $\langle K \rangle = \frac{1}{2}\langle \mathbf{x} \cdot \mathbf{F} \rangle$ where $F_i = \partial V/\partial x_i$. Different methods of estimation may have different rates of convergence.

Since PIMC simulations provide only imaginary time correlation functions, $C(\mathrm{it})$, dynamical quantities cannot be obtained directly. Analytic continuation to real time should lead to the true dynamical correlation functions, $C(\mathrm{t})$. Unfortunately, the frequencies which dominate $C(\mathrm{it})$ and $C(\mathrm{t})$ are very different and unless statistical noise in $C(\mathrm{it})$ obtained from a PIMC simulation is very small, the transformation process can lead to serious errors. Maximum entropy (ME) methods have been found to be the

most convenient for handling this ill-conditioned 'inversion' problem [39, 40, 41]. However, ME methods have not yet been used extensively in conjunction with PI simulations for chemical systems and will not be reviewed here.

3. Monte Carlo methods

Monte Carlo methods require a positive weighting function $P(\mathbf{y})$ to be associated with every configuration $\mathbf{y}$ of the system of interest in order to evaluate averages of the form

$$\langle F \rangle = \frac{\int P(\mathbf{y})\, F(\mathbf{y})\, d\mathbf{y}}{\int P(\mathbf{y})\, d\mathbf{y}}. \tag{30}$$

Metropolis Monte Carlo methods generate a Markovian random walk through configuration space. The rules determining the random walk are set by defining a transition matrix $T(\mathbf{y} \rightarrow \mathbf{y}')$ and an acceptance probability $A(\mathbf{y} \rightarrow \mathbf{y}')$ where the transition matrix determines the probability with which the random walk will move from one configuration $\mathbf{y}$ to a neighbouring configuration $\mathbf{y}'$ and the acceptance probability determines whether such a move will be accepted. Provided the detailed balance condition

$$T(\mathbf{y} \rightarrow \mathbf{y}')\, A(\mathbf{y} \rightarrow \mathbf{y}')\, P(\mathbf{y}) = T(\mathbf{y}' \rightarrow \mathbf{y})\, A(\mathbf{y}' \rightarrow \mathbf{y})\, P(\mathbf{y}') \tag{31}$$

is satisfied, a sufficiently long random walk is guaranteed to generate a set of configurations distributed according to the probability function $P(\mathbf{y})$. The flexibility of Monte Carlo methods derives largely from the ability to manipulate the T and A matrices to ensure rapid convergence and ergodicity of the random walk. In the case of PI simulations, an additional degree of freedom computationally is provided by the fact that alternative representations of the path allow for different choices of the Metropolis variables. Consequently the vast majority of PI simulations have used Monte Carlo sampling techniques. The discretized and Fourier representations of the path are commonly used for atomic systems and are described in sections 3.1 and 3.2 respectively. Modifications to the discretized PI scheme required for simulations of bosonic systems are outlined in section 3.3. The recently developed restricted PIMC algorithm for many-fermion systems is described very briefly in section 3.4.

3.1. *Discretized representation of paths*

Representing paths as a set of positions at equally spaced points in imaginary time is referred to as the discretized path approximation. The short time propagator connecting two adjacent points on the path can be evaluated at several different levels of accuracy [26, 42, 43]. The more accurate the propagator, the fewer the number of discrete positions which must be specified in order to evaluate the action accurately and lower the number of auxilliary variables that must be sampled in the Monte Carlo procedure. However, this increase in efficiency owing to the reduced dimensionality of the partition function may be offset by the increased computational cost of evaluating a more accurate propagator. In practice, the choice must be made based on various factors, such as the magnitude of quantum effects and the ease of evaluation of first and higher order derivatives of the potential. Generally the smaller the quantum effects, the simpler the choice of the propagator can be.

The least accurate representation of the short time/high temperature propagator is the primitive approximation which is adequate for quasiclassical systems such as solid argon. However, as quantum effects increase, the degree of discretization or the

Trotter index must be increased to maintain accuracy. Since the harmonic force constant between adjacent beads on the quantum polymer is $mM/\beta\hbar^2$, increasing the Trotter index results in increasingly stiff harmonic links and the computational problem of ensuring the ergodicity of the Metropolis walk becomes intractable. It is therefore useful to use more accurate expressions for the high temperature propagator and reduce the degree of discretization required for adequate convergence. A number of different strategies have been developed for generating short time propagators of different levels of accuracy. We focus on those which appear to be the most useful for atomic systems. The primitive approximation

$$\exp(-\varepsilon\hat{H}) \approx \exp(-\varepsilon\hat{K})\exp(-\varepsilon\hat{V}) \tag{32}$$

has an error of the order ε^2. The symmetrized form of the primitive approximation [26, 44]

$$\exp(-\varepsilon\hat{H}) \approx \exp(-0{\cdot}5\varepsilon\hat{V})\exp(-\varepsilon\hat{K})\exp(-0{\cdot}5\varepsilon\hat{V}) \tag{33}$$

has an error of the order of ε^3. When this symmetrized form is incorporated in the partition function we obtain

$$\mathrm{Tr}\{\exp(-\varepsilon M(\hat{K}+\hat{V}))\} = \mathrm{Tr}\{[\exp(-\varepsilon\hat{K})\exp(-\varepsilon\hat{V})]^M\} + \mathcal{O}(M\varepsilon^3). \tag{34}$$

The next higher order of approximation is given by

$$\mathrm{Tr}\{\exp(-\varepsilon M(\hat{K}+\hat{V}))\} = \mathrm{Tr}\{[\exp(-\varepsilon\hat{K})\exp(-\varepsilon\hat{V}_{\mathrm{eff}})]^M\} + \mathcal{O}(M\varepsilon^5) \tag{35}$$

where $\hat{V}_{\mathrm{eff}} = \hat{V} + (\beta/24M)[\hat{V},[\hat{K},\hat{V}]]$. In the coordinate representation,

$$\hat{V}_{\mathrm{eff}}(\mathbf{x}) = V(\mathbf{x}) + (\beta^2\hbar^2/24mM^2)\sum_{i=1}^{N}\left(\frac{\partial V}{\partial x_i}\right)^2 \tag{36}$$

where the second term is a quantum correction to the bare potential $V(\mathbf{x})$ [44]. Since this quantum correction is proportional to the sum of the squares of the forces acting on the particles, it can be readily evaluated for most atomic systems. While higher order correction terms to the propagator have been derived formally, they become increasingly more expensive to evaluate and therefore have not been used widely, except in the context of lattice systems.

An alternative strategy is to take advantage of the fact that the pair potential approximation is often very good for atomic and molecular systems. Let the action associated with going from point $\mathbf{x}$ to point $\mathbf{x}'$ in time ε along a path be denoted by $S(\mathbf{x}, \mathbf{x}'; \varepsilon)$. Then the potential energy contribution to the action is defined as $U(\mathbf{x}, \mathbf{x}'; \varepsilon) = S(\mathbf{x}, \mathbf{x}'; \varepsilon) - \ln \rho_{\mathrm{fp}}(\mathbf{x}, \mathbf{x}'; \varepsilon)$ where ρ_{fp} is the free particle density matrix. Within the pair potential approximation and provided three-body and higher order correlations are small, one can write $U(\mathbf{x}, \mathbf{x}'; \varepsilon) \approx \Sigma_{i<j} u(x_{ij}, x'_{ij}; \varepsilon)$ where $u(x_{ij}, x'_{ij}; \varepsilon)$ is connected to the density matrix for a pair of atoms. The accurate evaluation of the pair density matrix, while expensive, needs to be done only once at the start of the simulation. The pair action approach has been used very successfully for simulating liquid and solid helium. In all discretized path integral Monte Carlo (DPIMC) methods, the Metropolis variables are the positions of the $3NM$ beads. The probability weights associated with a given configuration will, however, depend on the choice of the high temperature propagator.

Even with improved high temperature propagators, the problem of ensuring adequate sampling of configuration space by collective motions of the polymers remains. An intuitively appealing path for circumventing this difficulty comes from

considering the normal modes of the quantum polymer [38, 45]. In the absence of an interation potential, all Cartesian degrees of freedom of the system are decoupled. For a single degree of freedom, the harmonic intrapolymer potential is given by $V_p = (mM/2\beta\hbar^2)\sum_{l=1}^{M}(x_l - x_{l+1})^2$. Diagonalization of the second derivative matrix of this potential leads to the normal coordinates, $\{Q_k\}$, $k = 1$ to M,

$$Q_k = (1/M^{1/2})\sum_{l=1}^{M} x_l \exp(2\pi i k l/M). \tag{37}$$

In the normal mode representation, the kinetic energy contribution to the path action from a single degree of freedom will be

$$\int_0^{\beta\hbar} \frac{m}{2}\left(\frac{\mathrm{d}x(u)}{\mathrm{d}t}\right)^2 \mathrm{d}u = \frac{2mM}{\beta\hbar^2}\sum_{k=1}^{M} |Q_k|^2 \sin^2(\pi k/M). \tag{38}$$

Thus the kinetic energy term is written as a sum of contributions from independent normal modes. The zero-frequency mode, $k = 0 = M$, corresponds to motion of the centre of mass of the polymer and makes no contribution to the kinetic energy. All normal modes, other than the zero frequency mode, are Gaussian distributed with variance $\sigma_k^2 = \beta\hbar^2/4mM\sin^2(\pi k/M)$ for a free particle. The potential energy term will couple these normal modes and cause distortions from the free particle distribution. The low frequency modes will correspond to large, collective motions of all beads of the polymer while the high frequency modes will cause small, local path fluctuations. The normal modes can now be used as Metropolis variables and the displacements scaled according to the Gaussian dispersions associated with each normal mode.

3.2. *Fourier representation of paths*

The Fourier PI approach introduces a set of auxiliary variables which represent different length scale fluctuations of the quantum paths instead of a discrete set of points on the path [46–48]. All paths contributing to a density matrix element $\rho(\mathbf{x}_i, \mathbf{x}_f; \beta)$ have the same initial point $\mathbf{x}_i$ at $u = 0$ and final point $\mathbf{x}_f$ at $u = \beta\hbar$. The classical path for a free particle is just the straight line: $\mathbf{x}_c(u) = \mathbf{x}_i + (\mathbf{x}_f - \mathbf{x}_i)(u/\beta\hbar)$. All other paths can be expressed as fluctuations $\mathbf{y}(u)$ about the classical free particle path as $\mathbf{x}(u) = \mathbf{x}_c(u) + \mathbf{y}(u)$ where $\mathbf{y}(u) = 0$ at $u = 0$ and $u = \beta\hbar$. Given the boundary conditions on $\mathbf{y}(u)$, we can expand the displacement for a Cartesian coordinate i as a Fourier sine series

$$y_i(u) = \sum_{k=1}^{\infty} a_{i,k}\sin(k\pi u/\beta\hbar) \tag{39}$$

where the Fourier series can be truncated at some values $k_{\max}$. The $3Nk_{\max}$ Fourier coefficients are the auxilliary variables necessary to describe the quantum paths contributing to the PI. By suitably differentiating $\mathbf{x}(u)$ and substituting in equation (10)

$$S(\mathbf{x}(u)) = \frac{m(\mathbf{x}_f - \mathbf{x}_i)^2}{2\beta\hbar^2} + \sum_k \frac{\mathbf{a}_k^2}{2\sigma_k^2} + \beta V_{\mathrm{eff}} \tag{40}$$

where $\sigma_k^2 = 2/\beta\hbar^2/mk^2\pi^2$, $V_{\mathrm{eff}} = (1/\beta\hbar)\int_0^{\beta\hbar} V(\mathbf{x}(u))\,\mathrm{d}u$ and $\mathbf{a}$ is the set of kth order Fourier coefficients for all the particles. Therefore

$$Z = J\int \mathrm{d}\mathbf{x}\,\mathrm{d}\mathbf{a}\exp\left(-\sum_k \frac{\mathbf{a}_k^2}{2\sigma_k^2} - \beta V_{\mathrm{eff}}\right). \tag{41}$$

J is the Jacobian associated with the transformation from $\mathscr{D}(\mathbf{x}(u)) \rightarrow \mathrm{d}\mathbf{a}$ and can be evaluated by considering the free particle limit, i.e. $J = \rho_{\mathrm{fp}}(\mathbf{x}, \mathbf{x}; \beta)(\Pi_k (2\pi\sigma_k^2)^{1/2})$. The Metropolis variables are now the $3N$ spatial coordinates $\mathbf{x}$ and the $3Nk_{\max}$ Fourier coefficients. The Fourier path integral Monte Carlo (FPIMC) approach is similar in spirit to the normal mode approach in that it decouples the kinetic energy term into contributions from $3Nk_{\max}$ independent degrees of freedom. In addition, the path fluctuations associated with a Fourier coefficient of order k are proportional to σ_k and therefore decrease as $1/k$. In contrast, in the normal mode approach they decrease as $1/\sin(\pi k/M)$ which is much less rapid.

A computationally very efficient version of the FPIMC algorithm, known as partial averaging, can be obtained by approximately integrating out the very short wavelength, high frequency Fourier modes. Let the Fourier coefficients be divided into two sets, those with $k \leqslant k_{\max}$ and those with $k > k_{\max}$. Therefore a cyclic path in imaginary time can be written as

$$\mathbf{x}(u) = \mathbf{x}_1 + \sum_{k=1}^{k_{\max}} \mathbf{a}_k \sin(k\pi u/\beta\hbar) + \sum_{k>k_{\max}}^{\infty} \mathbf{b}_k \sin(k\pi u/\beta\hbar). \tag{42}$$

If $k_{\max}$ is chosen to be sufficiently large, then all Fourier modes with $k > k_{\max}$ will be associated with very short length scale displacements and may be regarded as effectively decoupled from the potential. Then these Fourier coefficients with $k > k_{\max}$ may be regarded as purely Gaussian variables with variance σ_k^2. This would imply that any linear combination $p = \Sigma_k \lambda_k b_k$ of such Gaussian variables should correspond to a Gaussian variable p with variance $\Sigma_k \lambda_k^2 \sigma_k^2$. Therefore,

$$x_\lambda(u) = \mathbf{x}_1 + \sum_{k=1}^{k_{\max}} \mathbf{a}_k \sin(k\pi u/M) + p \tag{43}$$

where p is a Gaussian variable with variance

$$\sigma^2(u) = \sum_{k>k_{\max}} \sigma_k^2 \sin^2(k\pi u/\beta\hbar) = \frac{\beta\hbar^2}{m}\left[u(1-u) - \frac{2}{\pi^2}\sum_{k=1}^{k_{\max}} \frac{\sin^2(k\pi u/\beta\hbar)}{k^2}\right]. \tag{44}$$

Therefore we can write

$$Z = J\int \mathrm{d}\mathbf{x}\,\mathrm{d}\mathbf{a} \exp\left(-\sum_{k=1} \frac{a_k^2}{2\sigma_k^2}\right) \langle \exp(-\beta V_{\mathrm{eff}})\rangle_{\mathrm{G}} \tag{45}$$

where $\langle \exp(-\beta V_{\mathrm{eff}})\rangle_{\mathrm{G}}$ is the Gaussian average

$$\int \mathrm{d}\mathbf{b} \exp\left(-\sum \frac{b_k^2}{2\sigma_k^2} \exp(-\beta V_{\mathrm{eff}}(\mathbf{x}(u)+p)\right) = \int \mathrm{d}p \exp\left(-\frac{p^2}{2\sigma^2(u)}\right) \exp(-\beta V_{\mathrm{eff}}(\mathbf{x}(u)+p), \tag{46}$$

where $\mathbf{x}(u)$ is now a path defined by the lower order Fourier coefficients. Using the Gibbs–Boguliobov inequality, one can write

$$\int \mathrm{d}p \exp\left(-\frac{p^2}{2\sigma^2(u)}\right) \exp(-\beta V_{\mathrm{eff}}(\mathbf{x}(u)+p)) \geqslant \exp\left(-\beta \int \mathrm{d}p \exp\left(-\frac{p^2}{2\sigma^2(u)}\right) V_{\mathrm{eff}}(\mathbf{x}(u)+p)\right). \tag{47}$$

For any multidimensional system one can show that the RHS of the above inequality can be evaluated to second order in p as

$$V_p(\mathbf{x}(u)) = (1/\beta\hbar)\int_0^{\beta\hbar} du\,(V(\mathbf{x}(u)) + \sum_{i=1}^{3N} 0{\cdot}5\sigma^2(u)\,V_{ii}(\mathbf{x}(u)) \tag{48}$$

where $V_{ii}(\mathbf{x}(u))$ is a diagonal element of the second-derivative matrix, or the Hessian, evaluated $\mathbf{x}(u)$. Therefore the partial averaging strategy replaces the path average of the bare potential by the path average of a quantum corrected potential. The partial averaging version of the FPIMC has been shown to be efficient for a number of atomic systems. For example a comparison of FPIMC and DPIMC simulations for the $(para\text{-}H_2)_{13}$ cluster at 2·5 K shows that, for comparable errors bars, 32 auxilliary variables are required for convergence in the FPIMC scheme whereas 128 are required in the DPIMC scheme within the primitive approximation [49, 50]. Note that in the DPIMC method, the primitive approximation was coupled with the bisection path integral Monte Carlo (BPIMC) method which is described in the next section.

3.3. *Bosonic systems*

The PI simulation of a bosonic system, particularly in the region of the Bose–Einstein transition, is a more difficult computational problem than the simulation of a system of interacting, distinguishable quantum particles. The methods described in sections 3.1 and 3.2 are efficient for boltzmannons but they require substantial elaboration to be effective for bosonic systems. Simulation techniques for bosonic systems have been developed mainly in the context of the discretized path integral formulation. While identical particle exchange can be incorporated in the FPIMC approach, this has so far been implemented only for model systems and is not discussed here [51].

The difficulty in simulating bosonic systems arises because of the discrete character of permutation space. A random walk based on a simple transition matrix involving transitions to neighbouring configurations will be ergodic in configuration space, provided simulation times are long enough, since any spatial path can be continuously deformed to any other path. This is, however, not true of permutational moves which will be frequently rejected unless accompanied by substantial reorganization of the spatial paths. Therefore an intelligent choice of the transition matrix must be made in order to generate trial permutation cum spatial moves with a reasonable acceptance probability. Several different methods have been devised to accomplish this and we shall focus on the most widely used approach: the BPIMC algorithm.

The bisection method attempts to construct trial paths given the endpoints $\mathbf{x}$ and $P\mathbf{x}$ by constructing the path in stages corresponding to successive bisections of the time interval from 0 to $\beta\hbar$. We discuss the logic of the bisection algorithm based on the primitive approximation to the partition function [52]. In actual simulations it is usually necessary to use more accurate representations of the short time propagator, for which details can be found in the very comprehensive review article by Ceperley [6].

The first step in the bisection method is to sample the trial permutation based on the free particle density matrix (see equation (15)). Since only a small fraction of the $N!$ possible permutations will have significant probability at any finite temperature, therefore a table of probabilities of different permutations can be constructed and some trial permutation P can be sampled. Once a trial permutation has been sampled, a trial path must be built up. The BPIMC method is based on the recognition that trial

paths are most likely to be rejected due to changes in the midpoint of the path since by definition the endpoints have a reasonable potential energy. The product rule property of the density matrix implies that

$$\rho(\mathbf{x}, P\mathbf{x}; \beta) = \int d\mathbf{x}_m \, \rho(\mathbf{x}, \mathbf{x}_m; \beta/2) \, \rho(\mathbf{x}_m, P\mathbf{x}; \beta/2). \tag{49}$$

Therefore the conditional probability Π_1 of sampling the midpoint $\mathbf{x}_m$ given endpoints $\mathbf{x}$ and $P\mathbf{x}$ at $u = 0$ and $u = \beta\hbar$ respectively, will be

$$\Pi_1(\mathbf{x}_m; \mathbf{x}, P\mathbf{x}) = \frac{\rho(\mathbf{x}, \mathbf{x}_m; \beta/2) \, \rho(\mathbf{x}_m, P\mathbf{x}; \beta/2)}{\rho(\mathbf{x}, P\mathbf{x}; \beta)} \tag{50}$$

where the subscript on Π denotes the first level of bisection. A similar bisection scheme can then be used to bisect the subintervals from 0 to $\beta\hbar/2$ and $\beta\hbar/2$ to $\beta\hbar$. If $M = 2^l$ discrete points are required to represent accurately the path action, then one needs l levels of bisection. Since

$$\rho(\mathbf{x}, P\mathbf{x}; \beta) = \int d\mathbf{x}_1 \, d\mathbf{x}_2 \ldots d\mathbf{x}_M \, \rho(\mathbf{x}, \mathbf{x}_1; \beta/M) \, \rho(\mathbf{x}_1, \mathbf{x}_2; \beta/M) \ldots \rho(\mathbf{x}_{M-1}, P\mathbf{x}; \beta/M) \tag{51}$$

we can rewrite using conditional probabilities

$$\rho(\mathbf{x}, P\mathbf{x}; \beta) = \rho(\mathbf{x}, P\mathbf{x}; \beta) \, \Pi_1(\mathbf{x}_{M/2}; \mathbf{x}, P\mathbf{x}) \, \Pi_2(\mathbf{x}_{M/4}; \mathbf{x}, \mathbf{x}_{M/2}) \, \Pi_2(\mathbf{x}_{3M/4}; \mathbf{x}_{M/2}, P\mathbf{x}) \ldots . \tag{52}$$

The BPIMC scheme therefore first tests the broad features of the path for acceptability and then builds up the short length scale features. The catch in this scheme is that the exact density matrix elements will not be available except for the final level of bisection when the high temperature semiclassical approximation is valid. However, since what is being sought is a physically reasonable transition matrix, an approximate form of the density matrix for higher values of β is sufficient. A convenient approximation is to set

$$\rho(\mathbf{x}_i, \mathbf{x}_f; u) \approx \pi(\mathbf{x}_i, \mathbf{x}_f; u) = \rho_{fp}(\mathbf{x}_i, \mathbf{x}_f; u) \exp(-0{\cdot}5u(V(\mathbf{x}_i) + V(\mathbf{x}_f)) \tag{53}$$

where ρ_{fp} is the free particle density matrix. This choice of π and the structure of equation (52) ensures that the conditional probabilities will cancel out in such a way as to leave the weights associated with a given configuration in Z_{NM} unchanged.

Now consider a segment of the path at level l of the bisection algorithm. The endpoints of the path are $\mathbf{x}_i$ at $u = n\beta/2^{l-1}$ and $\mathbf{x}_f$ at $u = (n+1)\beta/2^{l-1}$. The old value of the midpoint of this segment of the path is denoted by $\mathbf{x}_m$. The trial value of the midpoint $\mathbf{x}_t$ is sampled with probability

$$T_l(\mathbf{x}_t) = \frac{\rho_{fp}(\mathbf{x}_i, \mathbf{x}_t; \beta/2^l) \, \rho_{fp}(\mathbf{x}_t, \mathbf{x}_f; \beta/2^l)}{\rho_{fp}(\mathbf{x}_i, \mathbf{x}_f; \beta/2^{l-1})}. \tag{54}$$

It can be shown that if this trial midpoint is accepted with probability corresponding to $\min\{1, \exp(-(\beta/2^{l-1})(V(\mathbf{x}_t) - V(\mathbf{x}_t) - V(\mathbf{x}_m))\}$, then it is equivalent to selecting the midpoint with the appropriate conditional probability. If positions at any level of bisection are rejected, then one must go back to the initial step and attempt a new permutation. If positions at all levels are accepted, then the new path is accepted. The BPIMC scheme has been shown to be very useful for bosonic systems. It can also increase the efficiency of the standard DPIMC procedures for distinguishable particles.

3.4. *Fermionic systems*

The diagonal elements of the density matrix for a many-fermion system, $\rho_F(\mathbf{x}, \mathbf{x}; \beta)$, will be positive. The fermion 'sign' problem arises when one writes $\rho_I(\mathbf{x}, \mathbf{x}'; \beta) = (1/N!)\Sigma_P \xi^P \rho_D(\mathbf{x}, P\mathbf{x}'; \beta)$ and attempts to sample over the permutations. A viable Monte Carlo method can be devised if one can rearrange terms to keep only positive contributing paths to the diagonal density matrix elements. A possible solution to this problem has recently been suggested by the restricted PI identity [10, 53]. Consider a density matrix element $\rho(\mathbf{x}, \mathbf{x}^*; \beta)$, which must be a solution to the Bloch equation

$$-\frac{\partial \rho}{\partial \beta} = \hat{H}\rho, \tag{55}$$

with initial condition

$$\rho(\mathbf{x}, \mathbf{x}^*; 0) = (1/N!)\sum_P \xi^P \delta(\mathbf{x} - P\mathbf{x}^*). \tag{56}$$

At a time $t = \beta\hbar$ the density matrix element will have nodal surfaces which carve the space into nodal cells. The Bloch equation can be solved within each nodal cell by using the appropriate initial condition and zero boundary conditions at $t = \beta$ on the nodal surface. This will be equivalent to restricting the PI to be a sum over node-avoiding paths such that $\rho(\mathbf{x}, \mathbf{x}^*; t)$ has the same sign for all t lying between 0 and β. The diagonal density matrix can be written as

$$\rho_F(\mathbf{x}, \mathbf{x}; \beta) = \int d\mathbf{x}^* \, \rho_F(\mathbf{x}, \mathbf{x}^*; 0)\, \rho_F(\mathbf{x}^*, \mathbf{x}; \beta). \tag{57}$$

Writing $\rho_F(\mathbf{x}^*, \mathbf{x}; \beta)$ as a sum over node-avoiding paths, results in only positive contributions from the product $\rho_F(\mathbf{x}, \mathbf{x}^*; 0)\, \rho_F(\mathbf{x}^*, \mathbf{x}; \beta)$ to the diagonal density matrix element. Therefore if the exact nodes of the density matrix are known, one could sample paths by adapting the standard bosonic PI algorithm so as to ensure that the sampling was restricted to node-avoiding paths. In practice, one does not know the exact nodes and some suitable approximation must be used. For example, free particle nodes were used in the simulations of normal liquid ^{3}He [54]. The restricted path integral Monte Carlo (RPIMC) method has also been used to study ^{3}He–^{4}He mixtures [55] and hydrogen plasma [56].

4. Molecular dynamics

Dynamical schemes for sampling the configuration space of the classical system isomorphic to the quantum N-body system can be devised. The prefactor $(m/2\pi\varepsilon\hbar^2)^{3NM/2}$ in equation (12) corresponds to the integral over the momenta of NM classical particles obeying Maxwell–Boltzmann statistics at temperature ε. Therefore by introducing NM classical particles, each of fictitious mass m'_j and momentum p'_j, one can write a Lagrangian

$$\mathscr{L} = \sum_{j=1}^{3NM} \frac{p_j'^2}{2m'_j} - \frac{m}{2\varepsilon\hbar^2}\sum_{i=0}^{M-1}(\mathbf{x}_i - \mathbf{x}_{i+1})^2 - \frac{1}{M}\sum_{i=0}^{M-1} V(\mathbf{x}_i), \tag{58}$$

and generate a molecular dynamics scheme for sampling the configurational integral [23, 24]. While configurational averages will be exactly the same as those obtained from a Monte Carlo scheme, the dynamics will be entirely fictitious and unrelated to the true quantum dynamics. Like all molecular dynamics schemes, collective motion through configuration space may be somewhat more facile than for Monte Carlo schemes. However, such path integral molecular dynamics (PIMD) algorithms have several disadvantages: quantum statistics cannot be incorporated, ergodicity is

problematic, especially for high Trotter numbers, and efficient higher order propagators cannot be easily used. Therefore PIMD schemes have been much less used than PIMC schemes. Recently, however, PIMD algorithms have been revived, in the context of *ab initio* PI simulations, since they can be coupled very efficiently with Car–Parinello (CP) codes for obtaining the ground electronic states [28–35]. However, for such combined PIMD-CP algorithms to be efficient, several elaborations are necessary, including transformation to normal modes, multiple timestep molecular dynamics and separate thermostatting of individual beads of the quantum polymers by Nosé–Hoover chains.

5. Applications to atomic and molecular systems

5.1. *Solvated electrons*

The solvated electron, a 'free' electron trapped in a cavity formed by solvent molecules, plays an important role in a variety of chemical phenomena and was one of the first systems to be studied using PIMC simulations [57–59]. The structure of a solvated electron in a fluid will be determined by the competition between two factors: a tendency to delocalize and occupy as large a volume as possible in order to minimize the kinetic energy and a tendency to minimize potential energy by optimizing electron–solvent interactions. In the case where the dominant contribution to the electron–solvent interaction is an excluded volume or repulsion interaction, the electron will tend to localize in regions of low fluid density. If the attractive interactions can be enhanced in these low density traps (for example, by the presence of oriented solvent dipoles) then the size of the cavity can be reduced substantially. PI simulations of an excess electron in a variety of fluids has led to a reasonable understanding of the complex interplay between various factors which determines the localized versus delocalized character of the electronic states and the associated changes in solvent structure. For example, helium behaves as expected on the basis of a hard sphere electron–solvent interaction; conversely, the much larger polarizability of the xenon atom results in a much more attractive e^-–Xe interaction and results in the electron being localized on high density clusters rather than low density traps [60]. Studies on branched and chain alkanes indicate that the details of the electron–solovent pseudopotential, such as the degree on anisotropy, significantly affect electron mobility as a function of density [61].

The hydrated electron has been shown to be a transient species of crucial importance in solution photochemistry since its identification more than 30 years ago [62, 63]. PIMC simulations of the hydrated electron indicate that the electron is characterized by a localized density distribution of approximately 2 Å radius. Analysis of the solvent structure shows that the solvent is bond oriented, rather than dipole oriented, with respect to the excess electron. Recent PIMC studies have concentrated on electron attachment to water clusters [64].

The solvated electron is central to the metal–insulator transitions observed in alkali metal–ammonia solutions and related systems, which have a long experimental history [59]. The localized versus extended states responsible for the metal–insulator transition with increasing alkali metal concentration have been the subject of several simulation studies. The dilute limit is ideally treated by PIMC methods [65]. The results show the trapping or localization of single electrons in solvent cavities of an effective size of about 4 Å. The results of the simulation agree well with experiment as well as with predictions of the reference interaction site model (RISM) polaron theory [58]. The metallic limit with high electron concentration can be treated by CP methods [66–68]. The intermediate regime, specially where spin pairing occurs, can be treated

by both approaches. In the spin pairing regime, the simulations show that electron pairs form singlet states which occupy a peanut-shaped cavity with the two peaks in the electron density separated by 7 Å. The triplet state is unstable with respect to the singlet state by approximately 0·6 eV.

5.2. *Quantum solids and liquids*

Simple atomic solids and liquids bound by van der Waals interactions are ideal systems for comparing the results from PIMC simulations against experimental data since the interaction potentials are well parametrized. The magnitude of quantum effects can be varied from the near classical behaviour of xenon to the large quantum effects displayed by solid and liquid helium. Experimentally, the single particle kinetic energy distribution obtained from deep inelastic neutron scattering (DINS) is a good indicator of quantum character since deviations from the classical Maxwell–Boltzmann distribution increase with increasing quantum character. Other experimental indicators of quantum effects are, for example, specific heat capacities as a function of temperature, pair correlation functions from neutron scattering and isotope effects on lattice parameters.

The PIMC methods described in sections 3.1 and 3.2 work very well for atomic solids and liquids in the absence of identical particle exchange. Theoretical and experimental average kinetic energies of solid and liquid neon and helium agree to better than 5% over a wide range of temperatures and densities [69–71]. The isotope shift in the lattice constant of solid ^{20}Ne and ^{22}Ne has been computed to very high accuracy [72].

The most dramatic early success of the PIMC technique was the simulation of the Bose–Einstein condensation of liquid ^{3}He [10]. Agreement with experimental data was shown to be excellent; for example, the superfluid transition temperature was calculated to within 0·02 K of the experimental value. The RPIMC method discussed in section 3.4 has been applied to liquid ^{3}He and ^{3}He–^{4}He mixtures [54, 55].

5.3. *Clusters*

Clusters have attracted much attention by virtue of being small systems which bridge the transition from molecular to bulk properties [73, 74]. While clusters can show properties similar to those of bulk matter, for example collective behaviour analogous to a phase transition, they are sufficiently small to be studied at the same level of microscopic detail as molecular systems. Quantum clusters have been studied largely with a view to understanding finite size effects on phase transitions of quantum many-body systems. For example, the superfluid transition of liquid ^{4}He is a quantum phase transition whose cluster analogue is accessible both experimentally and computationally. PI simulations of ^{4}He droplets of 64 and 128 atoms reveal a superfluid transition broadened by finite size effects [75]. While large, ultracold helium clusters can be produced in supersonic jets, unequivocal experimental proof of the superfluidity of helium clusters is not yet available. Since near helium clusters are hard to probe spectroscopically, the strategy has been to dope the clusters with a suitable chromophore, such as SF_6 or an alkali atom [76–78]. Rotationally resolved spectroscopy of SF_6 in helium clusters containing approximately 4000 atoms indicates a cluster temperature of about 0·4 K. Simulations of SF_6He_N clusters indicate that the relatively high binding energy of SF_6 reduces the superfluid fraction in comparison with pure helium clusters but the doped cluster should have a superfluid fraction greater than 0·7 by 0·4 K [79].

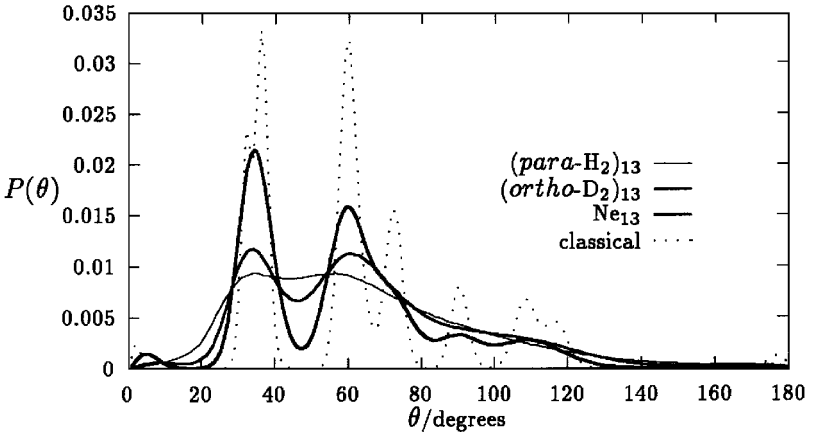

Figure 1. Comparison of the angular distribution functions of (*para*-H_2)$_{13}$, (*ortho*-D_2)$_{13}$ and Ne_{13} from PIMC simulations (see [49]). The simulations were performed at a reduced temperature of $k_B T/\varepsilon = 0{\cdot}073$ where ε is the well depth of the pair potential. The Lennard-Jones parameters for the three systems are very similar. The angular distribution function derived from a classical Monte Carlo simulation of Ne_{13} is also shown. The peaks at 36° and 60° are characteristic features of the icosahedral symmetry shown by small Lennard-Jones clusters.

No substance, other than liquid helium, undergoes a bulk superfluid transition. However, since *para*-H_2 is known to form a quantum solid with a very high zero point energy, it offers the interesting possibility that in a cluster the melting temperature can be lowered sufficiently that superfluidity can occur. This possibility was tested by Sindzingre *et al.* using PIMC simulations of *para*-H_2 molecules [80]. They showed that 13 and 18 molecule clusters exhibit a significant probability of non-identity permutations but such exchanges are considerably suppressed in clusters containing 33 or more molecules.

Clusters can exhibit a finite system analogue of bulk melting. Unlike the bulk, clusters possess distinct and separate freezing T_f and melting T_m points; between T_f and T_m, the cluster exists in dynamical equilibrium between solid-like and liquid-like forms. While clusters cannot obviously possess long range translational order characteristic of solids, the Lindemann index (the root mean square bond length fluctuation) can be used to monitor the cluster solid–liquid transition (CSLT); on melting, this quantity increases sharply from a value of about 7% or less for the solid-like phase to about 30% for the liquid-like cluster. The CSLT is most pronounced for magic number clusters which display a significantly greater binding energy per atom than their neighbouring size clusters. Such magic number clusters have a potential energy surface in which the global minimum is energetically well separated from a range of closely spaced metastable minima; the solid-like phase is associated with localization in the global minimum. Quantum effects on the CSLT in such magic number systems have been extensively studied by PIMC methods. The lowering of the transition temperature, T_f and T_m, owing to quantum effects, has been demonstrated for several systems such as H_2, D_2 and Ne clusters [81–85]. Figure 1 shows the differences in the angular distribution functions of (*para*-H_2)$_{13}$, (*ortho*-D_2)$_{13}$ and Ne_{13} clusters. At the simulation temperature, *ortho*-D_2 and *para*-H_2 may be regarded as spherically symmetric, pseudo-atomic species with pair potential parameters very similar to those of neon; therefore, differences in structure can be attributed largely to quantum

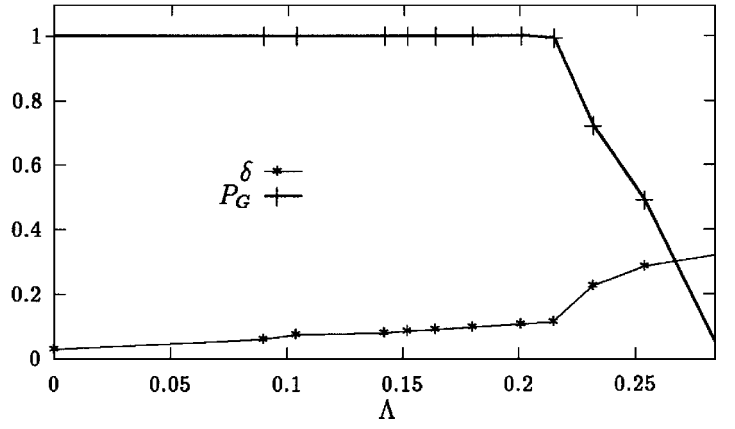

Figure 2. The probability of occupancy of the global minimum P_G as a function of the de Boer parameter Λ. For a nineteen particle Lennard-Jones cluster (see [86]). The de Boer parameter is a measure of the extent of quantum effects on the system and is defined as $\Lambda = \hbar/\sigma(m\varepsilon)^{1/2}$ where ε and σ are the well depth and size parameters of the pair potential respectively and m is the particle mass. P_G is an indicator of the solid-like character of the cluster. The results are for a constant reduced temperature $k_B T/\varepsilon = 0{\cdot}1$. The sharp fall in P_G over a relatively narrow range in Λ is indicative of a quantum delocalization-induced cluster solid–liquid transition analogous to the thermal melting of such systems.

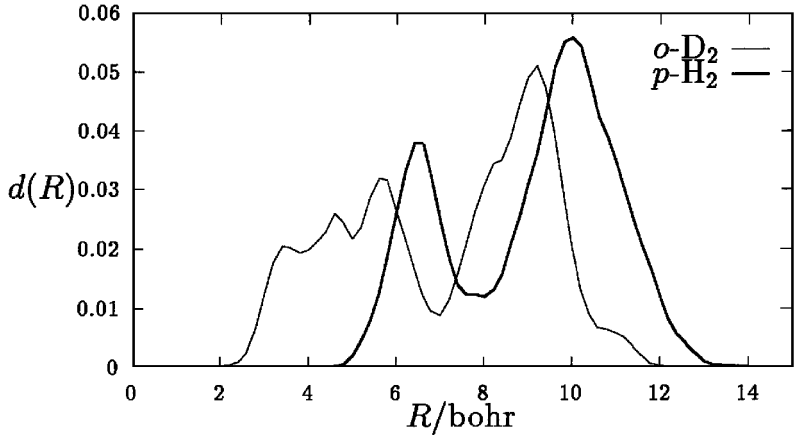

Figure 3. Radial density profiles $d(R)$ for the two isotopic species in $(para\text{-}H_2)_9$ $(ortho\text{-}D_2)_9$ at 2·5 K (see [88]). The localization of the heavier isotope in the core is evident.

effects. In addition, the kinetic energy increase associated with quantum delocalization has been shown to play an analogous role to the thermal kinetic energy and can be shown to induce a quantum fluctuation induced CSLT [86, 87] (see figure 2).

PIMC simulations have predicted some rather unusual quantum analogues of bulk phase transitions. For example, FPIMC simulations have demonstrated that in an isotopically mixed quantum cluster, the heavier isotope will be preferentially localized in the core and the lighter one on the surface [88, 89]. An example of this type of isotopic segregation is shown in figure 3 for the $(ortho\text{-}D_2)_9(para\text{-}H_2)_9$ cluster. A variation on this theme of species segregation in clusters is provided by mixed clusters of *ortho*- and *para*-D_2 where the *para*-D_2 entity is preferentially localized in the core

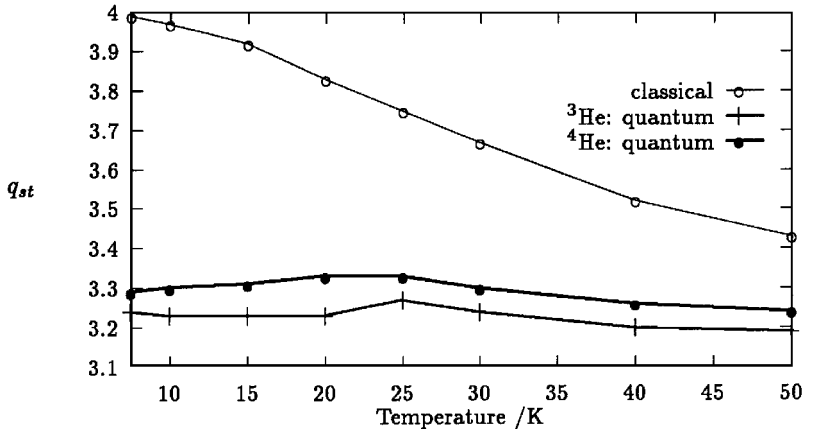

Figure 4. Isosteric heats of adsorption (in kJ mol^{-1}) for helium in silicalite in the dilute limit when interparticle interactions are negligible. Classical and quantum simulation results for the two helium isotopes are shown.

because at low temperatures only the *para*-D_2 species samples the anisotropic quadrupolar interaction in addition to the isotropic component common to both species [90].

The *ab initio* PI simulation techniques, discussed in section 2.3, have been applied to a number of ionic clusters of considerable chemical interest. For example, the structure of CH_5^+ has long been controversial with arguments that it is a unique carbonium ion as opposed to the theory that it is the prototype for a non-classical hypercoordinate carbocation with a ground state dominated by 3-centre–2-electron bonding. The PIMD simulations indicated that the quantum ground state is dominated by the latter configuration [28, 30]. Similar studies of the relative influence of thermal and quantum fluctuations have been carried out on $C_2H_3^+$, $H_5O_2^+$ and $H_3O_2^-$ [29, 32, 35]. The effect of protonation on $(H_2)_n$ clusters has also been studied by these methods [36].

5.4. *Orientational transitions*

Orientational transitions in molecular solids are associated with an increase in orientational degrees of freedom with temperature [13]. A molecule can be in more than one orientationally distinct position in a lattice site. For many molecular solids, the low temperature form has both long range orientational and translational order. As the temperature is increased, reorientational transitions can be sufficiently rapid to produce an orientationally disordered crystal of higher symmetry. On further heating, melting accompanied by loss of long range positional order sets in. (For highly anisotropic molecules, on heating positional disorder may set in earlier than orientational disorder resulting in formation of liquid crystals.) If the moments of inertia of the molecular rotors are small and the transition temperatures are low, then quantization of rotational motion will have observable consequences, such as change in transition temperatures with isotopic substitution. Obvious candidates for displaying orientational transitions of quantum rotors are solids of molecular hydrogen, hydrogen halides, methane and their deuterated analogues.

While the PIMC methods described in sections 2 and 3 could in principle be used for molecular solids, they prove very inefficient in simulating orientational transitions

since they do not take into account the fact that translational and intramolecular vibrational modes are effectively frozen. To develop a PIMC method for a system of interacting quantum rotors, it is necessary to evaluate the density matrix element $\langle \omega | \exp(-\varepsilon \hat{K}_{\mathrm{rot}} | \omega \rangle'$ where ω and ω' are angular coordinates and $\hat{K}_{\mathrm{rot}}$ is the rotational kinetic energy operator. This quantity can be evaluated numerically by inserting a suitable set of rotational wavefunctions, such as an asymmetric rotor basis for a nonlinear rotor and a spherical harmonic basis for a linear rotor. An additional complication is introduced by nuclear spin statistics which can determine the relative occupancy of rotational levels belonging to different irreducible representations of the point group of the molecular rotor. For example, the *para*-H_2 molecule has antiparallel nuclear spins and can occupy levels only with even values of the rotational angular momentum quantum number. Therefore at low temperatures *para*-H_2 exists in only the ground, $J = 0$ rotational state and behaves as a spherically symmetric bosonic entity. The *ortho*-H_2 molecule, in contrast, can occupy only odd rotational levels. It becomes therefore necessary to obtain representations of the density matrix element in accordance with the molecular point group. Non-identity representations are then found to have negative contributions which must be circumvented by fixed-node approximations. PIMC simulations of orientational transitions have been implemented for solid H_2–D_2 and solid CH_4 [91, 92].

5.5. *Surface adsorption*

Classical simulations of surfaces and interfaces is by now a well developed field [93]. Appreciable quantum effects can, however, be expected for light adsorbates, for example H_2, He, Ne, N_2 and CO, especially at low temperatures. One of the first surface adsorption problems to be studied by the PIMC method was ^{3}He and ^{4}He adsorption on graphite [94]. The quantum simulations corroborated experimental results for the different phase diagrams of the two isotopes and provided interesting insights into the microstructure associated with different phases. H_2 and D_2 at low temperatures also behave as pseudo-atomic adsorbates and most studies have concentrated on positional ordering transitions. Recently PIMC methods have been applied to study helium adsorption in porous media such as zeolites (see figure 4) [95].

In contrast to atomic substrates, diatomic molecules can exhibit a range of orientational transitions analogous to those seen in three-dimensional solids. The PI formulation for two-dimensional rotors is mathematically quite different from the three-dimensional case discussed in section 5.4. A viable PI simulation algorithm for such systems was developed by Nielaba, Marx and co-workers and applied to a number of systems. For example, N_2–graphite shows a herringbone transition; PIMC simulations have quantified that the lowering of the transition temperatures owing to quantum effects is 10% (30 K) [96]. The CO–graphite system is analogous to the N_2 adsorption problem except for a heat capacity anomaly at approximately 5 K. Recent PIMC simulations have shown that this must correspond to the head-to-tail ordering transition for the two-dimensional CO system [97]. Apart from specific molecular adsorbates, simulations of two-dimensional quantum rotor arrays reveal a quantum fluctuation induced disordering of orientationally ordered physisorbates which shows re-entrant behaviour [98].

5.6. *Rates of quantum processes*

An important dynamical quantity which can be approximately obtained from PI simulations is the rate constant for a quantum process. The quantum analogue of

classical transition state theory expresses the rate constant as a product of two factors: a dynamical factor ν and the probability $P(\mathbf{x}^*)$ of finding a quantum path with the path centroid $\mathbf{x}^* = (1/\beta\hbar)\int_0^{\beta\hbar}\mathbf{x}(u)\,du$ located at the transition state geometry [99]. The frequency of a reactive event will then be proportional to the probability of finding a tunnelling path which connects the reactant and product potential energy wells. The fraction of imaginary time spent in the barrier region along such a path will be small because the potential energy in the barrier region is high. This type of rapid process or instanton is then said to correspond to a kink in the quantum path. $P(\mathbf{x}^*)$ will be proportional to $\exp(-\beta\Delta F)$, where ΔF is the free energy required to create kinked paths. Thermodynamic integration techniques can be used to evaluate $P(\mathbf{x}^*)$ from PIMC simulations. The dynamical factor has a weak temperature dependence and cannot be obtained from a PI simulation; it can be approximated on the basis of classical simulations. This form of quantum transition state theory has been applied to calculate rates for quantum processes such as electron transfer, proton transfer, hydrogen diffusion and hydrogen chemisorption [100–102]. An ambitious application of this approach has been in explaining some of the unusual features of the primary electron transfer step in bacterial photosynthesis [103].

6. Concluding remarks

The implications of the quantum classical isomorphism, derived from the PI representation of the density matrix, for setting up Monte Carlo and molecular dynamics simulations analogous to those for classical many-body systems have been presented. An overview of PIMC and PIMD techniques has been provided with a view to illustrating how the efficiency and versatility of these techniques can be increased by appropriate choice of high temperature propagators, path representations and transition matrices. An attempt has been made to indicate the potential range of applicability of such computational tools by considering specific examples of PI simulations. The development of RPIMC methods for many-fermion systems and of maximum entropy methods for extracting dynamical information from PI simulations may in the future remove two of the major limitations of finite-temperature QMC techniques.

Acknowledgements

I would like to thank the Department of Science and Technology, New Delhi for financial support (Grant No. SP/S1/H-36/94).

References

[1] Cicotti, G., Frenkel, D., and McDonald, I. R., (editors), 1987, *Simulation of Liquids and Solids* (Amsterdam: North-Holland).
[2] Allen, M. P., and Tildesley, D. J., 1987, *Computer Simulation of Liquids* (Oxford: Clarendon Press).
[3] Binder, K. (editor), 1992, *The Monte Carlo Method in Condensed Matter Physics* (Berlin: Springer).
[4] Ceperley, D. M., and Alder, B., 1986, *Science*, **231**, 555.
[5] Hammond, B. L., Lester, W. A., and Reynolds, P. J., 1994, *Quantum Monte Carlo Methods in Ab Initio Quantum Chemistry* (Singapore: World Scientific).
[6] Ceperley, D. M., 1995, *Rev. mod. Phys.*, **67**, 279.
[7] Ceperley, D. M., and Mitas, L., 1996, *Adv. Chem. Phys.*, **93**, 1.
[8] Mitas, L., 1996, *Comput. Phys. Commun.*, **96**, 107.
[9] Chakravarty, C., 1995, *Curr. Sci.*, **69**, 739.

[10] Ceperley, D. M., 1996, *Simulation in Condensed Matter Physics and Chemistry*, edited by K. Binder and G. Ciccotti (Berlin: Springer-Verlag).
[11] Szabo, A., and Ostlund, N. S., 1982, *Modern Quantum Chemistry* (New York: MacMillan).
[12] Labanowski, J. K., and Andzelm, J. W. (editors), 1991, *Density Functional Methods in Chemistry* (New York: Springer).
[13] Parsonage, N. G., and Stavely, L. A. K., 1987, *Disorder in Crystals* (Oxford: Clarendon Press).
[14] Chandler, D., 1991, *Liquids, Freezing and the Glass Transition*, edited by J. P. Hansen, D. Levesque and J. Zinn-Justin (Amsterdam: Elsevier).
[15] Liu, K., Brown, M. G., Saykally, R. J., Gregory, J. K., and Clary, D. C., 1996, *Nature*, **381**, 501.
[16] Feynman, R. P., 1948, *Rev. mod. Phys.*, **20**, 367.
[17] Feynman, R. P., and Hibbs, A. R., 1965, *Path Integrals and Quantum Mehcanics* (New York: McGraw-Hill).
[18] Feynman, R. P., 1972, *Statistical Mechanics* (Reading, MA: Addison-Wesley).
[19] Morita, T., 1973, *J. Phys. Soc. Jap.*, **35**, 98.
[20] Barker, J., 1979, *J. chem. Phys.*, **70**, 2914.
[21] Chandler, D., and Wolynes, P. G., 1981, *J. chem. Phys.*, **74**, 4078.
[22] Schweizer, K. S., Stratt, R. M., Chandler, D., and Wolynes, P. G., 1981, *J. chem. Phys.*, **75**, 1347.
[23] Parrinello, M., and Rahman, A., 1984, *J. chem. Phys.*, **80**, 860.
[24] De Raedt, B., Sprik, L. M., and Klein, M. L., 1984, *J. chem. Phys.*, **80**, 5719.
[25] Pollock, E. L., and Ceperley, D. M., 1984, *Phys. Rev.* B, **30**, 255.
[26] Negele, J. W., and Orland, H., 1988, *Quantum Many-Particle Systems* (Reading, MA: Addison-Wesley).
[27] Schulman, L. S., 1981, *Techniques and Applications of Path Integration* (New York: Wiley).
[28] Marx, D., and Parrinello, M., 1994, *Z. Phys.* B (Rapid Note), **95**, 143.
[29] Cheng, H.-P., Barnett, R. N., and Landman, U., 1995, *Chem. Phys. Lett.*, **237**, 161.
[30] Marx, D., and Parrinello, M., 1995, *Nature*, **375**, 216.
[31] Marx, D., and Parrinello, M., 1996, *Science*, **271**, 179.
[32] Marx, D., and Parrinello, M., 1996, *J. chem. Phys.*, **104**, 4077.
[33] Tuckerman, M. E., Marx, D., Klein, M. L., and Parrinello, M., 1996, *J. chem. Phys.*, **104**, 5579.
[34] Tuckerman, M. E., Ungar, P. J., Vonrosenvinge, T. R., and Klein, M. L., 1996, *J. phys. Chem.*, **100**, 12878.
[35] Tuckerman, M. E., Marx, D., Klein, M. L., and Parrinello, M., 1997, *Science*, **275**, 817.
[36] Stich, I., Marx, D., Parrinello, M., and Terakura, K., 1997, *Phys. Rev. Lett.*, **78**, 3669.
[37] Chakravarty, C. (unpublished).
[38] Cao, J., and Berne, B. J., 1993, *J. chem. Phys.*, **99**, 2902.
[39] Silver, R. N., Sivia, D. S., and Gubernatis, J. E., 1990, *Phys. Rev.* B, **41**, 2380.
[40] Gubernatis, J. E., Jarrell, M., Silver, R. N., and Sivia, D. S., 1991, *Phys. Rev.* B, **44**, 6011.
[41] Gallichio, E., and Berne, B. J., 1994, *J. chem. Phys.*, **101**, 9909.
[42] Suzuki, M., 1976, *Commun. Math. Phys.*, **51**, 183; 1977, *ibid.*, **57**, 193.
[43] De Raedt, H., and De Raedt, B., 1983, *Phys. Rev.* A, **28**, 3575.
[44] Takahashi, M., and Imada, M., 1984, *J. Phys. Soc. Jap.*, **53**, 3765.
[45] Runge, K., and Chester, G. V., 1988, *Phys. Rev.* B, **38**, 135.
[46] Doll, J. D., Coalson, R. D., and Freeman, D. L., 1985, *Phys. Rev. Lett.*, **55**, 1.
[47] Coalson, R. D., Freeman, D. L., and Doll, J. D., 1986, *J. chem. Phys.*, **85**, 4567.
[48] Doll, J. D., Freeman, D. L., and Beck, T. L., 1990, *Adv. Chem. Phys.*, **78**, 61.
[49] Chakravarty, C., 1995, *Molec. Phys.*, **84**, 845.
[50] Scharf, D., Martyna, G. J., and Klein, M. L., 1992, *Chem. Phys. Lett.*, **197**, 231.
[51] Chakravarty, C., 1993, *J. chem. Phys.*, **99**, 8038.
[52] Trivedi, N., 1993, *Computer Simulation Studies in Condensed-Matter Physics V*, edited by D. P. Landau, K. K. Mon and H.-B. Schuttler (Berlin: Springer-Verlag).

[53] CEPERLEY, D. M., 1991, *J. statist. Phys.*, **63**, 1237.
[54] CEPERLEY, D. M., 1992, *Phys. Rev. Lett.*, **69**, 331.
[55] BONINSEGNI, M., and CEPERLEY, D. M., 1995, *Phys. Rev. Lett.*, **74**, 2288.
[56] PIERLEONI, C., BERNU, B., CEPERLEY, D. M., and MAGRO, R. W., 1994, *Phys. Rev. Lett.*, **73**, 2145.
[57] HERNANDEZ, J. P., 1991, *Rev. mod. Phys.*, **63**, 675.
[58] CHANDLER, D., and LEUNG, K., 1994, *Annu. Rev. Phys. Chem.*, **45**, 557.
[59] THOMPSON, J. C., 1985, *Metal–Non-Metal Transitions*, edited by P. P. Edwards and C. N. R. Rao (London: Taylor and Francis).
[60] COKER, D. F., BERNE, B. J., and THIRUMALAI, D., 1987, *J. chem. Phys.*, **86**, 5689; SPACE, B., COKER, D. F., LIU, Z. H., BERNE, B. J., and MARTYNA, G., 1992, *J. chem. Phys.*, **97**, 2002.
[61] LIU, Z., and BERNE, B. J., 1993, *J. chem. Phys.*, **99**, 9054.
[62] ROSSKY, P. J., and SCHNITTKER, J., 1988, *J. phys. Chem.*, **92**, 4277.
[63] HART, E. J., and BOAG, J. W., 1962, *J. Am. Chem. Soc.*, **84**, 4090.
[64] LANDMANN, U., BARNETT, R. N., CLEVELAND, C. L., SCHARF, D., and JORTNER, J., 1991, *J. phys. Chem.*, **91**, 4890; BARNETT, R. N., LANDMANN, U., CLEVELAND, C. L., and JORTNER, J., 1987, *Phys. Rev. Lett.*, **59**, 811.
[65] SPRIK, M., IMPEY, R., and KLEIN, M. L., 1986, *Phys. Rev. Lett.*, **56**, 2326.
[66] DENG, Z., MARTYNA, G. J., and KLEIN, M. L., 1992, *Phys. Rev. Lett.*, **68**, 2496.
[67] MARTYNA, G. J., DENG, Z., and KLEIN, M. L., 1993, *J. chem. Phys.*, **98**, 555.
[68] DENG, Z., MARTYNA, G. J., and KLEIN, M. L., 1994, *J. chem. Phys.*, **100**, 7590.
[69] CUCCOLI, A., MACCHI, A., TOGNETTI, V., and VAIA, R., 1993, *Phys. Rev.* B, **47**, 14923.
[70] TIMMS, D. N., EVANS, A. C., BONINSEGNI, M., CEPERLEY, D. M., MAYERS, J., and SIMMONS, R. O., 1996, *J. Phys.: condensed Matter*, **8**, 6665.
[71] CEPERLEY, D. M., SIMMONS, R. O., and BLASDELL, R. C., 1996, *Phys. Rev. Lett.*, **77**, 115.
[72] MUSER, M. H., NIELABA, P., and BINDER, K., 1993, *Phys. Rev.* B, **51**, 2723.
[73] BERRY, R. S., 1994, *J. phys. Chem.*, **98**, 6910.
[74] WHALEY, K. B., 1994, *Int. Rev. Phys. Chem.*, **13**, 41.
[75] SINDZINGRE, P., KLEIN, M. L., and CEPERLEY, D. M., 1989, *Phys. Rev. Lett.*, **63**, 1601.
[76] BARTELT, A., CLOSE, J. D., FEDERMANN, F., QUAAS, N., TOENNIES, J. P., 1996, *Phys. Rev. Lett.*, **77**, 3525.
[77] STIENKEMEIER, F., HIGGINS, J., CALLEGARI, C., KANORSKY, S. I., ERNST, W. E., and SCOLES, G., 1996, *Z. Phys.* D, **38**, 253.
[78] HARTMANN, M., MILLER, R. E., TOENNIES, J. P., and VILESOV, A., 1995, *Phys. Rev. Lett.*, **75**, 1566.
[79] YONGKYUNG, K., CEPERLEY, D. M., and WHALEY, K. B., 1996, *J. chem. Phys.*, **104**, 2341.
[80] SINDZINGRE, P., CEPERLEY, D. M., and KLEIN, M. L., 1991, *Phys. Rev. Lett.*, **67**, 1871.
[81] RICK, R. W., LEITNER, D. L., DOLL, J. D., FREEMAN, D. L., and FRANTZ, D. D., 1991, *J. chem. Phys.*, **95**, 6658.
[82] FRANTZ, D. D., FREEMAN, D. L., and DOLL, J. D., 1992, *J. chem. Phys.*, **97**, 5713.
[83] CHAKRAVARTY, C., 1995, *J. chem. Phys.*, **102**, 956.
[84] SCHARF, D., MARTYNA, G. J., and KLEIN, M. L., 1993, *J. chem. Phys.*, **99**, 8997.
[85] SCHARF, D., KLEIN, M. L., and MARTYNA, G. J., 1992, *J. chem. Phys.*, **97**, 3590.
[86] CHAKRAVARTY, C., 1995, *J. chem. Phys.*, **103**, 10663.
[87] CHAKRAVARTY, C., and RAMASWAMY, R., 1997, *J. chem. Phys.*, **106**, 5564.
[88] CHAKRAVARTY, C., 1995, *Phys. Rev. Lett.*, **75**, 1727.
[89] CHAKRAVARTY, C., 1996, *J. chem. Phys.*, **104**, 7223.
[90] BUCH, V., 1994, *J. chem. Phys.*, **100**, 7610.
[91] POLLOCK, E. L., and RUNGE, K. J., 1994, *Physica* B, **197**, 180.
[92] MUSER, M. H., and BERNE, B. J., 1996, *Phys. Rev. Lett.*, **77**, 2638.
[93] NICHOLSON, D., and PARSONAGE, N. G., 1982, *Computer Simulation and Statistical Mechanics of Adsorption* (New York: Academic Press).
[94] ABRAHAM, F. F., and BROUGHTON, J. Q., 1987, *Phys. Rev. Lett.*, **59**, 64.
[95] CHAKRAVARTY, C., 1997, *J. phys. Chem.*, **100**, 1878.
[96] MARX, D., OPITZ, O., NIELABA, P., and BINDER, K., 1993, *Phys. Rev. Lett.*, **70**, 2908.
[97] MARX, D., SENGUPTA, S., NIELABA, P., and BINDER, K., 1994, *Phys. Rev. Lett.*, **72**, 262.
[98] MARX, D., SENGUPTA, S., and NIELABA, P., 1994, *Ber. Bunsenges. Phys. Chem.*, **98**, 525.
[99] VOTH, G. A., CHANDLER, D., and MILLER, W. H., 1989, *J. chem. Phys.*, **91**, 7749.

[100] MARCHI, M., and CHANDLER, D., 1991, *J. chem. Phys.*, **95**, 889.
[101] MILLS, G., and JONSSON, H., 1994, *Phys. Rev. Lett.*, **72**, 1124.
[102] MATTSON, T. R., and WAHNSTRÖM, G., 1995, *Phys. Rev.* B, **51**, 1885.
[103] MARCHI, M., GEHLEN, J. N., CHANDLER, D., and NEWTON, M., 1993, *J. Am. Chem. Soc.*, **115**, 4178.